

Collagen fiber orientation pattern, osteon morphology and distribution, and presence of laminar histology do not distinguish torsion from bending in bat and pigeon wing bones

John G. Skedros^{1,2}  and Madison S. Doutré¹

¹Bone and Joint Research Laboratory, George E. Whalen Department of Veterans Affairs Medical Center, Salt Lake City, UT, USA

²Department of Orthopaedic Surgery, The University of Utah, Salt Lake City, UT, USA

Abstract

Bone can adapt to its habitual load history at various levels of its hierarchical structural and material organization. However, it is unclear how strongly a bone's structural characteristics (e.g. cross-sectional shape) are linked to microstructural characteristics (e.g. distributions of osteons and their vascular canals) or ultrastructural characteristics [e.g. patterns of predominant collagen fiber orientation (CFO)]. We compared the cross-sectional geometry, microstructure and ultrastructure of pigeon (*Columba livia domestica*) humeri, and third metacarpals (B3M) and humeri of a large bat (*Pteropus poliocephalus*). The pigeon humerus is habitually torsionally loaded, and has unremodeled ('primary') bone with vessels (secondary osteons are absent) and high 'laminarity' because a large majority of these vessels course circularly with respect to the bone's external surface. *In vivo* data show that the bat humerus is also habitually torsionally loaded; this contrasts with habitual single-plane bending of the B3M, where *in vivo* data show that it oscillates back and forth in the same direction. In contrast to pigeon humeri where laminar bone is present, the primary tissue of these bat bones is largely avascular, but secondary osteons are present and are usually in the deeper cortex. Nevertheless, the load history of humeri of both species is prevalent/predominant torsion, producing diffusely distributed shear stresses throughout the cross-section. We tested the hypothesis that despite microstructural/osteonal differences in these pigeon and bat bones, they will have similar characteristics at the ultrastructural level that adapt each bone for its load history. We postulate that predominant CFO is this characteristic. However, even though data reported in prior studies of bones of non-flying mammals suggest that CFO would show regional variations in accordance with the habitual 'tension regions' and 'compression regions' in the direction of unidirectional habitual bending, we hypothesized that alternating directions of bending within the same plane would obviate these regional/site-specific adaptations in the B3M. Similarly, but for other reasons, we did not expect regional variations in CFO in the habitually torsionally loaded bat and pigeon humeri because uniformly oblique-to-transverse CFO is the adaptation expected for the diffusely distributed shear stresses produced by torsion/multidirectional loads. We analyzed transverse sections from mid-diaphyses of adult bones for CFO, secondary osteon characteristics (size, shape and population density), cortical thickness in quadrants of the cortex, and additional measures of cross-sectional geometry, including the degree of circular shape that can help distinguish habitual torsion from bending. Results showed the expected lack of regional CFO differences in quasi-circular shaped, and torsionally loaded, pigeon and bat humeri. As expected, the B3M also lacked CFO variations between the opposing cortices along the plane of bending, and the quasi-elliptical cross-sectional shape and regional microstructural/osteonal variations expected for bending were not found. These findings in the B3M show that uniformity in CFO does not always reflect habitual torsional loads. Osteon morphology and distribution, and presence of laminar histology also do not distinguish torsion from bending in these bat and pigeon wing bones.

Correspondence

John G. Skedros, Bone and Joint Research Laboratory, George E. Whalen Department of Veterans Affairs Medical Center, 5316 South Woodrow Street, Suite 200, Salt Lake City, UT 84107, USA. T: 801 747 1020; F: 801 747 1023; E: jskedrosmd@uosmd.com

Accepted for publication 18 February 2019

Article published online 29 March 2019

Key words: bat humerus; bat third metacarpal; bone; bone adaptation; bone remodeling; collagen orientation; cortical thickness; load history; laminarity; microstructure; osteons; pigeon humerus; strain; strain mode.

Introduction

Cortical bone of limb bones in most bird species studied thus far is predominantly composed of primary osteons that, by definition, have vascular canals that form during primary appositional bone formation (Enlow & Brown, 1957; Francillon-Vieillot et al. 1990; Currey, 2002; Skedros & Hunt, 2004; de Margerie et al. 2005; Marelli & Simons, 2014; Lee & Simons, 2015). These vascular canals can be classified into four categories based on their orientation relative to the external surface of a bone when sectioned transversely: circular (parallel to external surface); longitudinal (parallel to long axis of bone); radial (orthogonal to external surface); and oblique (all other orientations; Enlow & Brown, 1957; de Ricqlès et al. 1991; de Margerie, 2002). In a study of various limb bones of Mallard ducks, de Margerie (2002) developed a method for quantifying the proportion of circular canals [laminarity index (LI) = total area of circular canals/total vascular area]. Bones that likely experience prevalent/predominant ('habitual') torsion, such as the femur, humerus and ulna, exhibited a high LI, which means that they have a high proportion of circular canals. In a study of 168 long limb bones from 22 species of birds, de Margerie et al. (2005) argued that the presence of a large percentage of circular canals (forming 'laminar bone') help accommodate/resist shear stresses that are caused by torsional loading.

Additional and more recent studies have shown that laminar bone is common in birds, and there is now an abundance of data suggesting that the degree of laminarity can represent an adaptation of avian limb bones or bone regions for differences in habitual load histories (e.g. low LI for bending vs. high LI for torsion; de Margerie et al. 2002; Skedros & Hunt, 2004; Simons & O'Connor, 2012; Marelli & Simons, 2014; Lee & Simons, 2015; Frongia et al. 2018). However, almost nothing is known about the magnitude of shear due to torsion in bird limb bones. Consequently, it is only safe to say that laminar bone appears to be associated with characteristic geometric features: high diameter/cortical thickness ratio, circular mid-shaft cross-section, and obliquely oriented collagen fibers. In this perspective, we sought to examine wing bones of flying animals (pigeon and bat) for potential functional relationships between cross-sectional morphology and characteristics of microstructure (e.g. secondary osteon prevalence and LI) and ultrastructure [e.g. predominant collagen fiber orientation (CFO)].

In selected pigeon and bat bones, this study compares the most common 'types' of adaptive cross-sectional morphological designs; namely, those generally best suited for torsional loads vs. those suited for bending loads. Beam-like limb bone diaphyses that are adapted for torsional/

multidirectional loads tend to be quasi-circular in transverse section; hence, they have similar magnitudes of the moments of area along all axes [i.e. the second moments of area (inertia, I) are similar or equivalent along the major (I_{max}) and minor (I_{min}) axes] (de Margerie et al. 2005; Skedros, 2012; Marelli & Simons, 2014). In contrast, bones with flattened or quasi-elliptically shaped cross-sections, often with asymmetrical cortical thickness that causes asymmetry in I_{max} and I_{min} , are a common design in bones subjected to generally habitual unidirectional bending. This asymmetric design suggests that the greatest bending resistance is along the long axis of the cross-section. In turn, asymmetric cross-sectional shapes, in addition to concurrent regional differences in cortical thickness, have been shown in many beam-like bones to correlate with load predictability by enhancing bending in one direction (Bertram & Biewener, 1988; Cubo & Casinos, 1998; Skedros, 2012).

Variability in the strengths of correlations between LI and bone cross-sectional morphology in limb bones of various bird species led Simons and co-workers (Simons & O'Connor, 2012; Marelli & Simons, 2014) to conclude that this microstructural characteristic and cross-sectional geometry are not strongly coupled. However, these investigators did not measure variations in predominant CFO, which is an ultrastructural characteristic that has been shown in bones of many non-avian species to correlate strongly with a history of habitual unidirectional bending and thereby helps differentiate this from torsional loading (Skedros et al. 2009, 2013a). Two studies report data in bird limb bones showing that increased laminarity not only reflects increased circularly coursing vessels, but also correlates with increased oblique-to-transverse CFO with respect to the long axis of the bone (Skedros & Hunt, 2004; de Margerie et al. 2005). In studies of transversely sectioned limb bones of several terrestrial mammals and some birds, regional differences in predominant CFO have been shown to be adaptive in three general contexts: (i) oblique-to-transverse CFO as an adaptation for habitual compression; (ii) even greater amounts of transverse CFO as an adaptation for habitual shear; and (iii) predominantly longitudinal CFO (i.e. mostly aligned along the long axis of a limb bone) is an adaptation for habitual tension loading (Skedros et al. 2009, 2011, 2013a; Skedros, 2012). These differing relationships of CFO with the three strain modes (tension, compression, shear) are called 'strain-mode-specific' adaptations (Skedros et al. 2006); this helps avoid fracture by accommodating the differing mechanical demands in these strain modes (Skedros et al. 2006; Ebacher et al. 2007; Skedros, 2012; Tang et al. 2015).

When considering LI vs. predominant CFO variations within or between bones of the same animal, it is unclear if

primary vessel orientation controls the emergence of regional CFO patterns or if CFO patterns (tissue ultrastructural anisotropy) can be modified independently as extragenetic adaptations for specific load histories (Skedros & Hunt, 2004; Skedros et al. 2007a). This is an important consideration because laminar bone, although common in mammals, is not consistently present in bones that experience habitual torsion (Foote, 1916; de Ricqlès et al. 1991; Hofmann et al. 2014; Pratt et al. 2018). However, most prior studies that have considered the mechanical relevance of variations in laminarity have not examined characteristics of the bone matrix (e.g. regional distribution of CFO) that are known to be comparatively more strongly and consistently associated with specific adaptations that can help distinguish torsion from bending load histories. Therefore, the mechanisms and ultimate biomechanical consequences of mammal vs. bird differences in limb bone hierarchical organization are unclear. In these perspectives, the present study focuses on examining potential relationships between cross-sectional morphology and various microstructural/ultrastructural characteristics in limb bones of bats and pigeons.

We posed the following question: is there a universally adaptable histological characteristic that, regardless of vessel orientation or the presence of secondary osteons, can be modified to accommodate torsion/shear? We propose that regional variations in predominant CFO is a strong candidate for this characteristic because: (i) experimental data show that it plays an important role in imparting toughness for the different mechanical behaviors in each specific strain mode (Skedros, 2012); (ii) extensive data in mammalian bones show that plasticity in regional distribution of CFO occurs regardless of the presence or absence of secondary osteons (Skedros et al. 2004, 2009, 2011, 2013a); and (iii) data from ulnae of sub-adult and adult domesticated turkeys (Skedros & Hunt, 2004) suggest that predominant CFO might be more strongly influenced by load history while regional variations in laminarity might be strongly influenced by the rate of osteogenesis (de Margerie et al. 2004; Skedros & Hunt, 2004). This latter issue suggests that laminarity and CFO might not be strongly coupled in terms of their importance in effecting mechanical adaptation.

Hypotheses

We used humeri from gray-headed flying foxes and common pigeons to compare histomorphology and cross-sectional geometry of these habitually torsionally loaded bones vs. a bone experiencing habitual directionally consistent bending (bat third metacarpal, B3M). In contrast to these humeri, *in vivo* strain measurements have shown that during wing flapping the B3M is loaded in single-plane bending, with equivalent durations in the two alternating directions (Swartz & Middleton, 2008). Table 1 lists our predictions including these main hypotheses.

1. The predominant CFO of the humeri will be more oblique (in accordance with adaptations expected for diffusely distributed shear) than the CFO in the B3M.
2. The humeri will have quasi-annular/circular cross-sectional shapes when compared with the relatively less circular cross-sectional shape of the B3M, which also correlates with adaptation for torsion/shear in the humeri.
3. The humeri will have high *K*-values (thinner cortices relative to outer diameter) as a torsion/shear-related adaptation when compared with the relatively lower *K*-value of the B3M.
4. The humeri will have similar cortical thickness in all anatomical quadrants, reflecting their greater complexity loading compared with the asymmetric cortical thickness of the B3M, which would be the expected means for ensuring that the B3M preferentially bends in the dorsal-ventral direction.
5. The B3M will have similar CFO in the dorsal and ventral cortices, reflecting the fact that these cortices experience similar magnitudes and durations of tension and compression during wing flapping (this differs from nearly all other bones that have been studied that have directionally consistent bending – where the compression strains are greater and of longer duration than tension strains).

Additional between- and within-bone variations are also evaluated either statistically or descriptively.

Materials and methods

Microscopic analysis of ultramilled sections

Segments were cut transversely from the mid-diaphyses of these bones from adult animals: 14 pigeon humeri (*Columba livia domestica*; 380–400 g); nine bat humeri; and nine B3M (*Pteropus poliocephalus*; 700–850 g). The bat bones were obtained from the same animals used by Swartz et al. (1992). The segments remained undecalcified and unstained, and were embedded in polymethylmethacrylate (PMMA; Emmanual et al. 1987; Skedros et al. 2011). A 0.5-mm-thick section of the embedded bone was cut using a low-speed, diamond blade saw (Exact, Germany) and continuous water irrigation. Using an ultramiller (Reichart/Jung Ultramiller), one surface of the section was ultramilled to a high luster finish. The milled surface was mounted onto a glass slide with cyanoacrylate glue and then milled to a thickness of $100 \pm 5 \mu\text{m}$ (Skedros et al. 1996, 2011).

The ultramilled specimens were imaged using circularly polarized light (CPL) to analyze the predominant CFO within quadrants of each of the bones. The bone tissue within each cortical quadrant was analyzed in $50 \times$ images, and the analysis of gray levels in these images was performed using previously described methods (Skedros et al. 2011). This method quantifies differences in CFO by differences in transmitted light (unfiltered broadband white), where brighter gray levels represent more oblique-to-transverse CFO (compression or shear adapted) and darker gray levels represent more

Table 1 Predicted differences or variations between and within bones.

Between bone differences				Observed*	
1. CFO	Generally more oblique-to-transverse in the humeri (expected adaptation for shear/torsion)			Y	
2. Cross-sectional shape	Relatively annular in humeri (expected in habitual torsion) Asymmetric in the B3M [reflecting habitual dorsal-ventral (D-V) bending]			N	
3. I_{max}/I_{min} (relates to cross-section shape and bending resistance)	Lower values in the humeri (reflecting lack of preferential bending direction) Higher values in B3M [reflecting habitual dorsal-ventral (D-V) bending]			Y/N	
4. K-value (~ inverse of CA/TA)	Relatively higher in humeri (torsionally loaded bones generally have greater diameters but thinner cortices) Lower in the B3M (reflecting increased CA/TA for increased loads and greater bending in distal wing)			Y	
5. $J(I_{max} + I_{min})$ [relates to $Z_{pol} = (J)/(\text{cross-section radius})$]	Greater in the humeri (reflecting increased resistance to torsional loading)			Y	
6. 2nd osteonal bone (involves OPD and FASB)	Few or no 2nd osteons in the humeri More in the B3M (likely more microdamage-mediated remodeling because greater loads/strains in distal wing)			Y	
Within bone differences		Pigeon humerus (habitual torsion)	Bat humerus (habitual torsion)	B3M (habitual bending along D-V plane)	
7. Cortical thickness	Equivalent [†] in all regions (Y*)	Equivalent [†] in all regions (Y*)	Thinner in the D and V cortices [‡]		(N*)
8. CFO	Equivalent in all regions (Y)	Equivalent in all regions (Y)	Equivalent in D and V cortices because of equivalent strain modes; more oblique-to-transverse in neutral axis (Cr-Cd cortices) ^{‡,§}		(Y/N)
9. 2nd osteonal bone (involves OPD and FASB)	No 2nd osteons (Y)	Equivalent in all regions (Y)	Difference only between neutral axis region (Cr and Cd cortices) vs. bending plane ^{‡,§}		(N)
10. 2nd osteon size (On.Ar) (relates to osteon diameter)	No 2nd osteons (Y)	Equivalent in all regions (Y)	Difference only between neutral axis region (Cr and Cd cortices) vs. bending plane ^{‡,§}		(N)
11. 2nd osteon shape (On.Cr)	No 2nd osteons (Y)	Equivalent in all regions (Y)	Difference only between neutral axis region (Cr and Cd cortices) vs. bending plane ^{‡,§}		(N)

Main hypotheses are highlighted in gray.

2nd, secondary; B3M, bat third metacarpal; CA/TA, cortical area/total area (a measure of cross-sectional robustness); Cd, caudal; CFO, collagen fiber orientation; CPL, circularly polarized light; Cr, cranial; D, dorsal; FASB, fractional area of 2nd bone; On.Ar, osteon area; On.Cr, osteon circularity; OPD, 2nd osteon population density; V, ventral.

*Results observed in this study: 'Y' = yes, 'N' = No. 'Y/N' = the first statement is yes, the second is no; see text for details.

[†]'Equivalent' in the humeri are predictions based on expectations in bones subject to habitual torsion.

[‡]In the B3M, the dorsal (D) and ventral (V) cortices are in the plane of habitual bending during wing flapping. The cortices are predicted to be relatively thicker in the cranial-caudal (Cr-Cd) plane because this would help enhance bending in the dorsal-ventral (D-V) direction.

[§]Similar to #8, predictions 9–11 are based on microstructural adaptations for enhancing toughness in D-V cortices for equivalent strain modes vs. relatively more shear in Cr-Cd cortices [for details, see Keenan et al. (2017) and Skedros et al. (2013a)].

longitudinal CFO (tension adapted; Boyde & Riggs, 1990; Bromage et al. 2003; Skedros et al. 2011). Image gray levels are expressed as weighted mean gray levels (WMGL), which are used to express predominant CFO of each image (hence referred to as 'CFO-WMGL'). A calibration standard for expressing CFO-WMGL data in terms of an average degree of CFO with respect to the bone's long axis was not used because the methodology for this was not well developed at the time of our data collection (Spiesz et al. 2011; Warshaw et al. 2017). Consequently, we report relative differences in predominant CFO, in accordance with nearly all prior studies that have examined

this ultrastructural characteristic in terms of interpreting load history in limb bones.

A CFO-WMGL value was quantified for each image taken in the dorsal, ventral, cranial and caudal cortex of each section of the bat and pigeon bones. This was accomplished by obtaining a histogram of the gray levels of each image in ImageJ (v. 1.43, National Institutes of Health, USA; Rasband, 1997–2016) and then using these to calculate a WMGL using described methods (Bloebaum et al. 1997). In the context of comparisons between two regions of a bone along a habitual bending plane (e.g. a 'compression region' vs. a

'tension region'), significantly 'higher' CFO-WMGL values represent brighter image gray levels (brighter birefringence in CPL correlates with adaptation for compression). Brighter gray levels represent predominant CFO that is more oblique-to-transverse than the relatively more longitudinal (hence 'lower' CFO-WMGL values = darker gray levels) in the opposing tension-adapted region. Additional description of how CPL imaging can be used to detect CFO differences in plane-parallel thin sections of bone can be found in Boyde & Riggs (1990) and Bromage et al. (2003).

The nomenclature used to describe the quadrants of the sectioned bones included dorsal, ventral, cranial and caudal (Marelli & Simons, 2014). This contrasts with Swartz & Middleton (2008) who considered the cranial cortex as medial and the caudal cortex as lateral.

Secondary osteon population density (OPD), fractional area of secondary osteon bone (FASB, expressed as a percentage), and the cross-sectional area (On.Ar) and shape (On.Cr; osteon circularity) of individual secondary osteons were quantified for each digitized image using described methods (Skedros et al. 2009, 2013a; Keenan et al. 2017). ImageJ (v. 1.43, National Institutes of Health, USA; Rasband, 1997–2016) was also used to obtain the osteonal data. No osteons were excluded when obtaining the FASB data. Only complete secondary osteons were used to determine On.Ar and On.Cr. In the few instances when osteons were excluded from the analysis of On.Ar and On.Cr, the osteons were either incomplete or were those with dramatic irregularities as described previously (Skedros et al. 2007b, 2013b).

Each osteon chosen for quantification was then selected in Adobe Photoshop using the 'quick select' tool. The 'stroke' and 'fill' functions were then used to 'paint' each osteon. These images were subsequently opened in ImageJ where each painted osteon was individually selected with the 'wand selection' tool, and then the 'interpolation spline' function was applied to smooth the pixels at the periphery of the osteon, at which point each osteon was then measured. Without this step, extraneous pixels at the osteon periphery would have inadvertently been quantified, which would have led to errant data, especially adversely influencing On.Cr (Mears et al. 2014, 2015; Keenan et al. 2017).

For analyses of CFO-WMGL and all other histomorphological characteristics, each cortex of each bone was analyzed independently, and then re-analyzed after excluding the highly birefringent ('bright') ring that was often present along the endosteal surface (de Margerie et al. 2005). The entire cross-section of each bone was also examined to see if there are secondary osteons in regions that were not included in the areas sampled by the images taken of each bone. These additional observations are reported qualitatively.

Cross-section/geometric analysis and regional cortical thickness

A low-magnification image of the whole cross-section of each bone was obtained and was used to make macroscopic measurements, including cortical thickness and outer diameters (i.e. sub-periosteal breadths in the dorsal-ventral and cranial-caudal directions), cortical area, medullary area, and axes of second moments of area (I_{max} and I_{min}). To accomplish this, digitized images of each cross-section were manually modified in Adobe Photoshop by painting the area of bone black and the non-bone area white. Cortical thickness and cross-sectional geometric parameters were then analyzed in these edited images. Cortical thickness was measured at the dorsal, ventral, cranial and caudal cortices. Cortical area (CA), medullary area

(MA) and total area (CA + MA) were determined for each section. Second moments of area (I_{max} and I_{min} , which are the sum of areas multiplied by the square of a distance from an axis, giving units of mm^4), polar moment of area ($J = I_{max} + I_{min}$) and polar section modulus (Z_{pol} , mm^3) were also quantified for each section (excluding the medullary canal; Ruff, 2002; Lee & Simons, 2015). These parameters were quantified in ImageJ using the BoneJ extension (ImageJ v. 1.49, National Institutes of Health, USA; Rasband, 1997–2016). Z_{pol} is an estimate of torsional rigidity and average bone bending rigidity (Ruff, 2002; Lee & Simons, 2015), and this is calculated as J divided by half the maximum cranial-caudal breadth. Circularity and cortical thickness (K -values closer to 1.0 = thinner cortex) were calculated using the methods described by de Margerie et al. (2005).

Statistical analysis

Statistical analyses were performed using NCSS 10.0 (Hintze, 2015) and STATA 14.1 (StataCorp, 2015) software. The Kolmogorov–Smirnov test for normality was performed on each variable. Pearson or Spearman correlations were obtained for various comparisons within each bone type.

We approached multiplicity (multiplicity of hypotheses and comparisons) by combining several approaches. Multiplicity arises when multiple comparisons are made to answer a single research question. We first considered what our specific hypotheses were based on what constituted a separate research question. In Table 1, the main hypotheses are highlighted, and the specific characteristics involved in these and the other primary research questions are described below in the final two paragraphs of this section. Because each research question stands on its own, without the need to consider results from other separate questions, no multiple comparison adjustment from comparisons made in other questions should be performed (Dunnnett & Goldsmith, 2006; Dmitrienko et al. 2010). If within a specific hypothesis there were several possible statistical comparisons, we first considered the primary–secondary approach to multiplicity (Bender & Lange, 2001). If a specific comparison was best suited to answer the research question, then it was selected as the primary comparison. Given only one comparison is required, there is no need for a multiple comparison adjustment. The other comparisons were then selected as secondary, which are reported as exploratory or descriptive hypotheses (specifics described below). Because secondary hypotheses do not answer the research question, there is no need for a multiplicity adjustment for them. For normal data, ANOVA tests were used to compare data within and between each bone type (i.e. three types = pigeon humerus, bat humerus, and B3M). For non-normal data, Kruskal–Wallis tests were used.

For cortical thickness and each material characteristic that required several comparisons to answer the study questions, such as using four bone regions to test if bone region was associated with the outcome, a repeated-measures ANOVA was performed. This design was used to determine if there is an effect of region (dorsal, ventral, cranial, caudal) within each bone type in accordance with predictions based on habitual torsion vs. bending (bat and pigeon humeri, vs. B3M), or dorsal-ventral bending plane vs. neutral axis (cranial-caudal direction; B3M only; Table 1, predictions 7–11). This type of analysis was done because the four regions are from the same bone. To determine which regional differences were driving the association, we performed all possible paired-sample t -tests, and then adjusted the P -values for all possible pairwise comparisons using a correlated sample Hochberg multiple comparison

procedure. This is the Hochberg ordinary procedure extended to correlated comparisons by multiplying by a constant derived on how correlated the pairwise comparisons are. This maintains the nominal alpha at 0.05, where otherwise the Hochberg procedure is too conservative (Sankoh et al. 1997). In this context, the three bone types were considered independently, as these were used to address bone-specific questions. In the instance where there were two very closely related variables that apply to the same research question (e.g. osteon area and osteon diameter), then we selected a primary outcome variable (osteon area) and secondary outcome variable (osteon diameter). A similar example is cross-sectional shape (primary outcome, prediction #2) vs. I_{\max}/I_{\min} (secondary outcome, prediction #3). In these cases, the primary outcome was used to test a study hypothesis or prediction, and the secondary outcome is simply reported descriptively.

In a separate analysis, an ANOVA was conducted for between-bone comparisons to determine if significant characteristic-specific differences exist that would be expected for habitual torsion (both humeri) vs. bending (B3M; Table 1, predictions 1, 2 and 4–6). These characteristics included CFO-WMGL, which is considered a primary outcome variable and was averaged from the four regions for each bone, and several structural characteristics, including cross-sectional shape (relates to I_{\max}/I_{\min}), K -value (cortical thinness), and J ($= I_{\max} + I_{\min}$, and relates to Zpol); each of which is also considered a primary outcome variable. Other structural measures for between-bone comparisons that are reported descriptively include cortical area/total area (cortical robustness), cortical thickness, I_{\max} , I_{\min} , I_{\max}/I_{\min} and Zpol.

Results

Results are summarized in Tables 1–4 and Figs 1–3. As shown in Fig. 1, the larger size and greater cross-sectional robustness [i.e. cortical area/total area, (CA/TA)] of the humerus of adult gray-headed flying foxes is commensurate with their two–three times greater body mass when compared with adult pigeons.

The representative images shown in Figs 2 and 3 reveal high laminarity (a large majority of circularly coursing primary vascular canals) in the pigeon humerus. Although not quantified here, the high LI that results from the preponderance of circularly coursing primary vascular canals in this bone of this pigeon species is well described (Lee & Simons, 2015). Secondary osteons were not observed in any of the pigeon humeri sections. In contrast, the primary bone of the bat humerus has minor amounts of vascularity, and the primary bone in the B3M appears to be avascular. In contrast to the pigeon humeri, the bat humeri and B3M have secondary osteons in the mid-to-deeper portions of the cortices (Fig. 3). This likely reflects osteons that formed earlier in development.

Consistent with expectations of the histological/ultrastructural adaptation for habitual torsional loading, there were no significant regional CFO-WMGL differences (with or without the inclusion of endosteal bone) within bat and pigeon humeri (Table 2). In addition, as expected when compared with the B3M, these habitually torsionally loaded bones (also with substantial concurrent shear and tension;

Swartz et al. 1992; Swartz & Middleton, 2008) had generally and significantly higher CFO-WMGL (presumed to be indicative of diffusely distributed prevalent/predominant shear). All three bones had significantly different CFO-WMGL from each other ($P < 0.01$).

Consistent with predictions, in the bat humeri there are no significant regional differences in cortical thickness (Table 2). The relatively minor cortical thickness variations in the bat humeri did not correlate with FASB ($r = 0.18$, $P = 0.27$). However, these cortical thickness variations have a low positive correlation with CFO-WMGL ($r = 0.32$, $P < 0.05$). In the pigeon humeri (which lack secondary osteons), cortical thickness also shows no significant regional differences (as expected) and, in this bone, there was no correlation between cortical thickness and CFO-WMGL. Additional geometric data for these humeri and the B3M are reported below.

Consistent with our expectations, the dorsal and ventral cortices of the B3M have similar thickness. However, contrary to our expectations, the cranial and caudal cortices (neutral axis region) of the B3M were not significantly thicker than the dorsal and ventral cortices (we expected that the dorsal and ventral cortices would be relatively thinner because they are aligned in the direction of habitual bidirectional bending). In the B3M, the relatively minor cortical thickness variations do not correlate with FASB ($r = -0.04$, $P = 0.8$) or CFO-WMGL ($r = 0.22$, $P = 0.2$).

Consistent with our expectations, the B3M has similar CFO-WMGL in the dorsal and ventral cortices (Table 2), which are in the plane of habitual bidirectional bending. However, the B3M does have a significant ventral vs. caudal CFO-WMGL difference, which is ~12% (means: 67.1 vs. 59.7, respectively; $P = 0.01$). The ventral vs. caudal CFO-WMGL difference is still statistically significant when the analysis was re-run after removal of the bright endosteal ring ($P = 0.05$). The results of all other within- and between-bone CFO/WMGL analyses also remained the same regardless of whether or not the endosteal bone was included in the analysis.

When considering all FASB data from all images in each bat bone, mean FASB (expressed as percentage) is substantially higher in the B3M than the bat humerus (18.1% vs. 2.8%; $P < 0.05$). This is consistent with predictions (Table 1, prediction #6).

However, contrary to our expectations in the B3M, OPD and FASB are distributed approximately equally among the four cortical regions. Also contrary to our expectations in the B3M, there are also no significant differences in On.Ar or On.Cr between the different cortices (Table 2).

Similar to the B3M and consistent with our expectations, the bat humerus had no significant regional differences in OPD, FASB or On.Cr. However, the bat humerus had greater On.Ar in the ventral and caudal cortices (mean diameter = 107 μm) compared with the dorsal and cranial cortices (mean diameter = 83 μm ; $P < 0.05$; Table 2).

Table 2 Cortical thickness and material characteristics by anatomical quadrants (means \pm standard deviations).

Species and location	Cortical thickness	CFO-WMGL	CFO-WMGL (excluding endosteal layer)	FASB (%)	OPD (no. per mm ²)	Osteon area (μm^2)	Osteon diameter (μm)	Osteon circularity (On.Cr)
A. Bat humerus								
Caudal (Cd)	0.81 \pm 0.2	87.6 \pm 9.2	85.1 \pm 14.3	4.8 \pm 5.9	5.4 \pm 5.9	6876 \pm 3587 ^{Cr,D}	108 \pm 32 ^{Cr,D}	0.93 \pm 0.05
Cranial (Cr)	0.81 \pm 0.3	89.6 \pm 9.6	84.5 \pm 14.7	1.3 \pm 1.8	3.2 \pm 5.1	4476 \pm 2752 ^{Cd,V}	83 \pm 30 ^{Cd,V}	0.95 \pm 0.03
Ventral (V)	0.75 \pm 0.2	84.6 \pm 11.4	82.8 \pm 14.3	4.4 \pm 3.4	2.9 \pm 3.0	7156 \pm 4320 ^{Cr,D}	106 \pm 35 ^{Cr,D}	0.95 \pm 0.04
Dorsal (D)	0.75 \pm 0.2	86.1 \pm 9.3	84.2 \pm 12.2	1.1 \pm 2.5	1.4 \pm 2.0	4111 \pm 2990 ^{Cd,V}	82 \pm 35 ^{Cd,V}	0.94 \pm 0.05
Entire section	0.78 \pm 0.2	87.0 \pm 9.7	84.1 \pm 13.4	2.8 \pm 3.6	3.2 \pm 4.4	6323 \pm 3754	101 \pm 34	0.94 \pm 0.05
B. B3M								
Caudal (Cd)	0.60 \pm 0.1	59.7 \pm 3.5 ^V	58.6 \pm 7.4 ^V	21.1 \pm 17.9	10.1 \pm 4.6	15 780 \pm 11 100	162 \pm 62	0.91 \pm 0.06
Cranial (Cr)	0.59 \pm 0.1	62.3 \pm 7.0	64.9 \pm 10.9	15.5 \pm 16.1	8.0 \pm 6.2 ^D	13 539 \pm 8485	156 \pm 52	0.89 \pm 0.05
Ventral (V)	0.58 \pm 0.1	67.1 \pm 5.2 ^{Cd}	66.2 \pm 3.5 ^{Cd}	19.1 \pm 13.4	17.1 \pm 11.1	16 492 \pm 9584	172 \pm 55	0.89 \pm 0.06
Dorsal (D)	0.67 \pm 0.2	63.2 \pm 6.3	62.0 \pm 10.4	16.8 \pm 13.2	14.7 \pm 6.4 ^{Cr}	16 383 \pm 10 468	166 \pm 60	0.91 \pm 0.04
Entire section	0.61 \pm 0.1	63.1 \pm 6.0	62.9 \pm 8.7	18.1 \pm 14.8	12.5 \pm 8.0	15 279 \pm 9744	163 \pm 56	0.90 \pm 0.06
C. Pigeon humerus								
Caudal (Cd)	0.45 \pm 0.1	112.2 \pm 8.7	110.6 \pm 9.6					
Cranial (Cr)	0.50 \pm 0.1	111.3 \pm 9.6	112.0 \pm 13.4					
Ventral (V)	0.47 \pm 0.1	113.3 \pm 13.8	116.0 \pm 13.3					
Dorsal (D)	0.49 \pm 0.2	113.4 \pm 9.8	114.4 \pm 11.3					
Entire section	0.48 \pm 0.1	111.8 \pm 10.6	113.2 \pm 11.8					

Superscripts indicate cortex where there is a significant difference within the bone, with a *P*-value < 0.05.

B3M, bat third metacarpal; CFO, collagen fiber orientation; FASB, fractional area of secondary osteon bone; OPD, osteon population density; WMGL, weighted mean gray level.

Table 3 Structural characteristics by quadrants (means \pm standard deviations).

Species and location	Circularity (1.0 = circle)	Cortical thinness (<i>K</i>) (1 = very thin wall)	Area (mm ²)	<i>I</i> _{max} (mm)	<i>I</i> _{min} (mm)	<i>I</i> _{max} / <i>I</i> _{min}	<i>J</i> (<i>I</i> _{max} + <i>I</i> _{min})	Zpol (mm ³)
A. Bat humerus*	0.95 \pm 0.02	0.68 \pm 0.04	22.1 \pm 6.4	27.8 \pm 15	24.9 \pm 12	1.13 \pm 0.09	52.7 \pm 29.0	18.5 \pm 7.9
B. B3M*	0.90 \pm 0.03	0.42 \pm 0.05	3.9 \pm 0.9	1.1 \pm 0.5	0.85 \pm 0.39	1.35 \pm 0.18	2.0 \pm 0.9	1.6 \pm 0.6
C. Pigeon humerus*	0.89 \pm 0.01	0.82 \pm 0.02	21.8 \pm 3.6	21.9 \pm 7.0	13.8 \pm 4.3	1.59 \pm 0.13	35.7 \pm 11.3	12.0 \pm 2.6

*When comparing the other structural characteristics included in this table (circularity, cortical thinness, area, *I*_{max}/*I*_{min}, *J* and Zpol), each bone was statistically significant from the other two bones in each characteristic, except for *I*_{max} and *I*_{min}, where there were no statistically significant differences between bat humerus and pigeon humerus. See additional details in text.

B3M, bat third metacarpal.

As expected, cortical thinness (*K*) shows the highest values (thinnest walls) in the humeri (pigeon > bat, *P* < 0.001) and lowest in the B3M (*P* < 0.001 for B3M vs. pigeon humerus; *P* < 0.001 for B3M vs. bat humerus; Table 3). These *K*-value differences mirror the differences in cortical robustness, which we expressed as cortical area/total area (CA/TA), and are significantly different (*P* < 0.001) between each bone type. The B3M has the highest average cortical robustness (0.82; as expected), the bat humerus is intermediate (0.53), and the pigeon humerus is lowest (0.33).

There are no significant differences in cranial-caudal vs. dorsal-ventral breaths (i.e. outer diameters) in any of the three bones. However, *I*_{max}/*I*_{min} showed statistically significant differences between each bone. The average

*I*_{max}/*I*_{min} values for the B3M, bat humerus and pigeon humerus are, respectively, 1.35, 1.13 and 1.59. These findings are contrary to our 'conventionally based' (Skedros, 2012) expectations (which we challenge below) that the habitually bent B3M would have the highest *I*_{max}/*I*_{min} values (hence enhanced bending rigidity in a particular direction). By contrast, we expected the torsionally loaded humeri would have *I*_{max}/*I*_{min} closer to 1.0 in both species (hence reflecting enhanced torsional rigidity). *I*_{min}, by being significantly lower in the pigeon humeri than the bat humeri (*P* < 0.01), accounts for the relatively higher-than-expected *I*_{max}/*I*_{min} ratios in the pigeon humerus when compared with the bat humerus.

Table 4 Correlation matrices (*r*-values), with *p* values listed below each *r*-value: (A) bat humerus, (B) B3M, (C) pigeon humerus.

A

	CFO-WMGL	Total area (mm ²)	Cortical thickness (K)	<i>I</i> _{max} / <i>I</i> _{min}	<i>J</i> (<i>I</i> _{max} + <i>I</i> _{min})	Circularity	FASB	CFO-WMGLe
CFO-WMGL	1.00							
	0.00							
Total area (mm ²)	0.71	1.00						
	0.02	0.00						
Cortical thickness (K)	0.05	-0.16	1.00					
	0.90	0.66	0.00					
<i>I</i> _{max} / <i>I</i> _{min}	-0.28	-0.28	0.36	1.00				
	0.43	0.44	0.30	0.00				
<i>J</i> (<i>I</i> _{max} + <i>I</i> _{min})	0.71	1.00	-0.16	-0.30	1.00			
	0.02	< 0.01	0.66	0.40	0.00			
Circularity	0.37	0.58	-0.52	-0.83	0.60	1.00		
	0.30	0.08	0.12	< 0.01	0.07	0.00		
FASB	0.28	0.56	-0.63	-0.42	0.59	0.73	1.00	
	0.43	0.10	0.05	0.23	0.07	0.02	0.00	
CFO-WMGLe	-0.55	-0.50	-0.55	-0.16	-0.54	0.11	-0.01	1.00
	0.10	0.14	0.10	0.66	0.11	0.76	0.98	0.00

B.

	CFO-WMGL	Total area (mm ²)	Cortical thickness (K)	<i>I</i> _{max} / <i>I</i> _{min}	<i>J</i> (<i>I</i> _{max} + <i>I</i> _{min})	Circularity	FASB	CFO-WMGLe
CFO-WMGL	1.00							
	0.00							
Total area (mm ²)	0.50	1.00						
	0.17	0.00						
Cortical thickness (K)	-0.71	-0.55	1.00					
	0.03	0.10	0.00					
<i>I</i> _{max} / <i>I</i> _{min}	0.57	0.14	-0.75	1.00				
	0.11	0.69	0.01	0.00				
<i>J</i> (<i>I</i> _{max} + <i>I</i> _{min})	0.49	1.00	-0.55	0.14	1.00			
	0.18	< 0.01	0.10	0.71	0.00			
Circularity	-0.65	-0.17	0.72	-0.96	-0.17	1.00		
	0.06	0.64	0.02	< 0.01	0.65	0.00		
FASB	-0.32	0.18	0.24	-0.47	0.19	0.67	1.00	
	0.40	0.64	0.53	0.20	0.62	0.05	0.00	
CFO-WMGLe	0.29	0.58	-0.30	-0.07	0.57	0.14	0.34	1.00
	0.45	0.10	0.44	0.85	0.11	0.72	0.38	0.00

C.

	CFO-WMGL	Total area (mm ²)	Cortical thickness (K)	<i>I</i> _{max} / <i>I</i> _{min}	<i>J</i> (<i>I</i> _{max} + <i>I</i> _{min})	Circularity	CFO-WMGLe
CFO-WMGL	1.00						
	0.00						
Total area (mm ²)	0.06	1.00					
	0.85	0.00					
Cortical thickness (K)	-0.48	0.36	1.00				
	0.08	0.21	0.00				
<i>I</i> _{max} / <i>I</i> _{min}	0.17	0.03	-0.23	1.00			
	0.56	0.92	0.44	0.00			

(continued)

Table 4. (continued)

C.

	CFO-WMGL	Total area (mm ²)	Cortical thickness (K)	I_{\max}/I_{\min}	$J(I_{\max} + I_{\min})$	Circularity	CFO-WMGL _e
$J(I_{\max} + I_{\min})$	0.15	0.98	0.17	0.08	1.00		
	0.61	< 0.01	0.57	0.78	0.00		
Circularity	0.26	0.12	0.17	-0.62	0.06	1.00	
	0.38	0.69	0.55	0.02	0.84	0.00	
CFO-WMGL _e	0.83	0.36	-0.17	0.24	0.41	0.08	1.00
	< 0.01	0.21	0.57	0.40	0.14	0.79	0.00

Highlighted cells indicate statistically significant correlations.

CFO, collagen fiber orientation; CFO-WMGL_e, WMGL not including the endosteal ring; FASB, fractional area of secondary osteon bone; WMGL, weighted mean gray level.

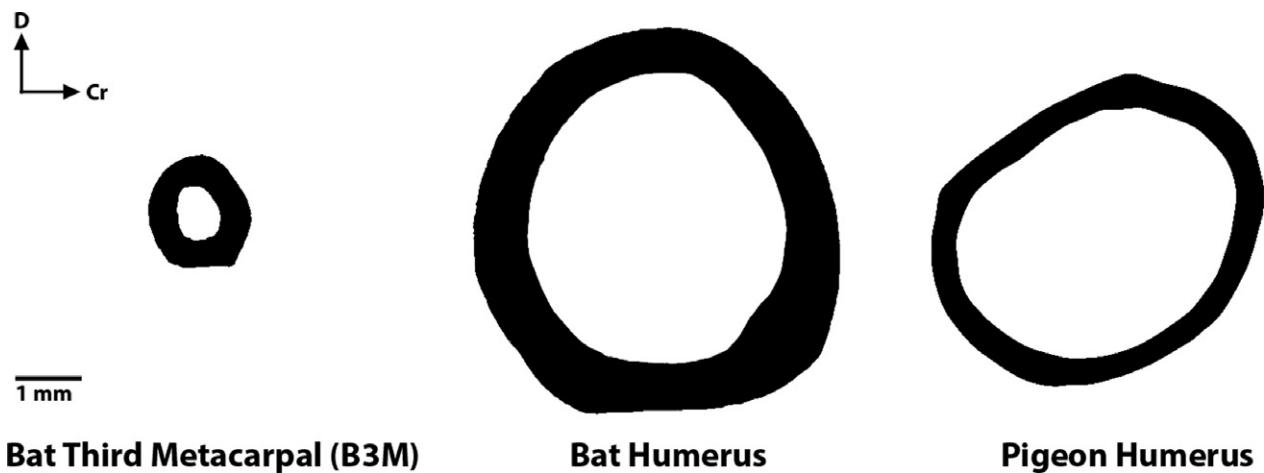


Fig. 1 Representative transverse cross-sections of the bat third metacarpal (B3M), bat humerus and pigeon humerus taken from low-magnification images of the whole cross-section of each bone. Each cross-section is set to the same scale to allow direct comparisons between them.

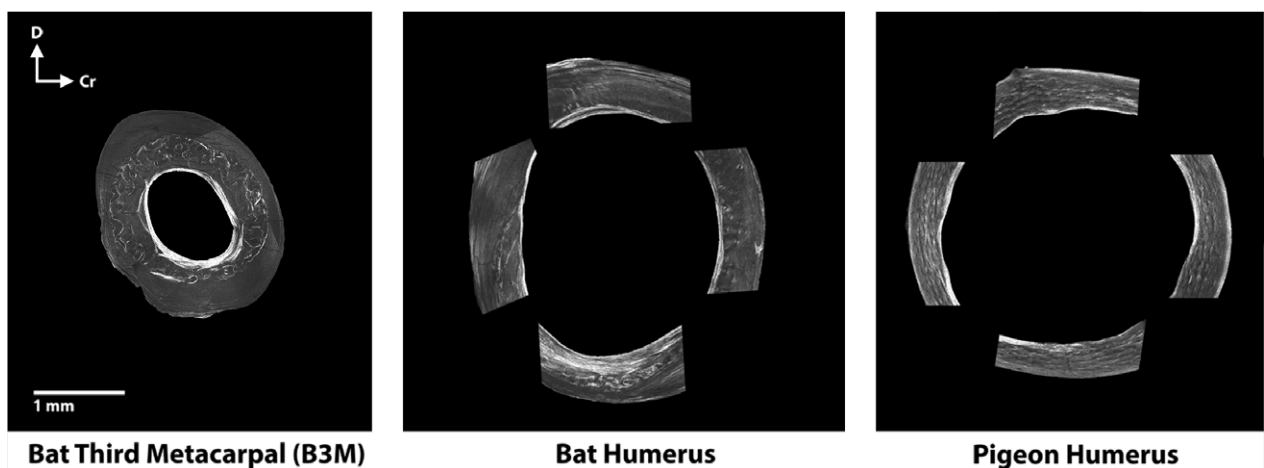


Fig. 2 Representative composite circularly polarized light (CPL) images of the bat third metacarpal (B3M), bat humerus and pigeon humerus. Images were obtained under the same illumination from polymethyl-methacrylate (PMMA)-embedded sections that were ultramilled to uniform thickness of $100 \pm 5 \mu\text{m}$. The sections were not stained and were not decalcified.

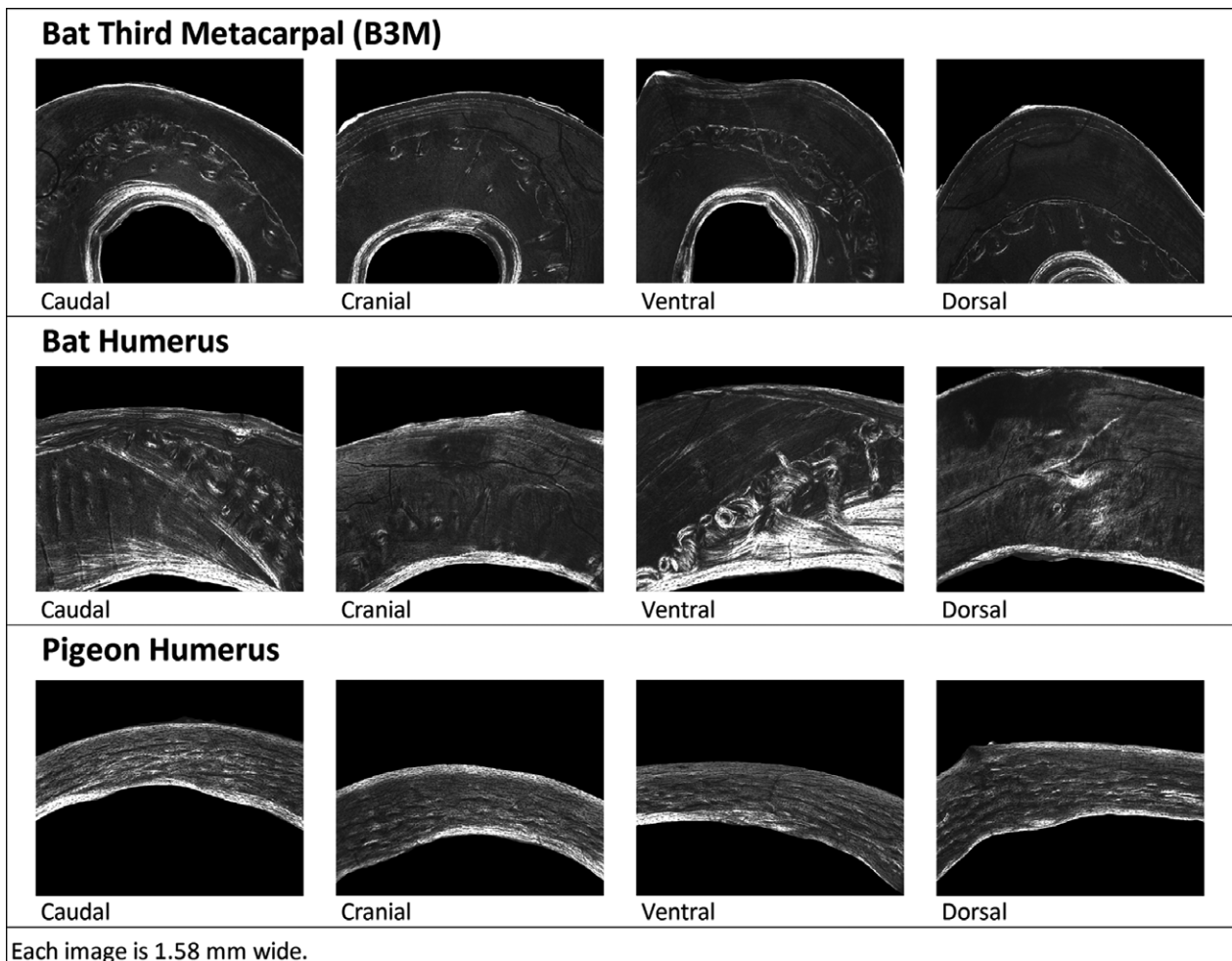


Fig. 3 Representative circularly polarized light (CPL) images taken from each bone in the caudal, cranial, ventral and dorsal quadrants. The breadth of each image is 1.58 mm. Images were obtained under the same illumination from polymethyl-methacrylate (PMMA)-embedded sections that were ultramilled to uniform thickness of $100 \pm 5 \mu\text{m}$. The sections were not stained and were not decalcified.

The I_{max} , I_{min} , J and Z_{pol} values of the B3M are significantly ($P < 0.01$) lower than the bat and pigeon humeri, which is not surprising (and was expected) given the large difference in external diameters of this bone when compared with the humeri. In contrast, and as expected, there is no significant difference in I_{max} ($P = 0.28$), I_{min} ($P = 0.11$), J ($P = 0.26$) and Z_{pol} ($P = 0.08$) between the bat and pigeon humeri. These data suggest that the bat and pigeon humeri have greater torsional rigidity than the B3M.

Discussion

Lack of laminar bone in bats suggests that variations of this histological type cannot be 'the universal tissue-level adaptation' for strain mode

In vivo strains measured on humeri of large bats (gray-headed flying foxes, *P. poliocephalus*) throughout the

wing-flapping cycle show that the diaphysis of this bone habitually experiences torsion (Swartz et al. 1992; Swartz & Middleton, 2008). As a consequence of torsion, these bones experience relatively higher, and more diffusely distributed, shear strains when compared with bones that, although have similar magnitudes of end-loads, are habitually loaded in bending where shear stresses are concentrated near the neutral axis region (Swartz & Middleton, 2008; Skedros, 2012). These findings in the humeri of these large bats are comparable to the *in vivo* strain environment of the diaphysis of the humerus of the common pigeon during flapping flight (Biewener & Dial, 1995). Similar to bat humeri, pigeon humeri also have quasi-circular cross-sectional shapes and thin walls, supporting the idea that these features are macrostructural adaptations for flight-induced torsion (Curry & Alexander, 1985; Marelli & Simons, 2014; Pratt et al. 2018). However, across a wide range of phylogeny, feeding

behavior and body size, bats lack laminar bone that is common in the humeri of pigeons as in many other avian species that also experience habitual torsion (de Margerie et al. 2005; Lee & Simons, 2015). In fact, the humeri of small-to-medium bodied bats (~6–100 g) are essentially avascular (Lee & Simons, 2015). In contrast, the primary bone of the humerus of the large-bodied bat *Pteropus vampyrus* is sparsely vascularized (Lee & Simons, 2015). Contrary to the avian-based hypothesis that wing bones habitually loaded in torsion contain predominantly circular canals, the primary bone of long bones in wings of this larger bat species (~1000 g) not only have comparatively fewer vessels, but these vessels also have a predominantly longitudinal to slightly radial orientation with respect to the long axis of the bone (Lee & Simons, 2015). In the setting of similar cross-sectional geometry of these torsionally loaded humeri of flying birds and a flying mammal, this difference in histological organization appears to confound straightforward interpretations of load history.

Is predominant CFO the universal tissue-level adaptation for strain mode?

The results of the present study show that the bat and pigeon humeri do not have regional variations in CFO-WMGL, which is consistent with the expected adaptation for diffusely distributed shear stresses throughout a section of a bone that is loaded in habitual torsion (Skedros et al. 2009, 2013a). This finding in bones with and without primary vascular tissue is an important advance for comparative histomorphological studies. This is because our results also show that variations in vascular patterns that characterize the high laminarity (i.e. increased proportions of circular coursing vessels) that occur in the pigeon humerus (Lee & Simons, 2015) and are believed to represent tissue-level optimization for habitual torsion in birds (de Margerie, 2002; de Margerie et al. 2005) cannot be the universal adaptation for torsionally loaded bones in animals that have roughly similar body sizes. The notable example reported here is the absence of laminar bone in the highly torsionally loaded bat humerus even though it resembles the habitual loading and cross-sectional shape of the pigeon humerus and many other torsionally loaded humeri of flying birds where laminar bone is common (de Margerie et al. 2005; Marelli & Simons, 2014; Lee & Simons, 2015; Frongia et al. 2018; Pratt et al. 2018).

Based on findings of our past studies of limb bones that lack laminar histology (Skedros, 2012; Skedros et al. 2013a, 2016b; Keenan et al. 2017), we concluded that variations in CFO represent the proximate, and perhaps universal, means for adapting cortical bone at the tissue level for the non-uniform strain-mode distribution of bending and for the diffusely distributed shear strains produced by torsion. Even in bones that naturally form prevalent secondary osteons, there are several examples showing that

secondary osteons are not needed for the expression of these adaptations (Mason et al. 1995; Skedros & Kuo, 1999; Skedros, 2012). In these cases, the primary bone that forms has preferred matrix orientation; hence, the adaptation is based on *de novo* bone formation via the modeling process and is not based on the renewal/reconstruction in small units seen in osteonal remodeling. For example, fibrolamellar bone (i.e. similar to the primary vascular bone described herein but also has a parallel-fibered bone component; Almany Magal et al. 2014) formed during growth has been shown to have the capacity to manifest regional variations in predominant CFO for non-uniform strain-mode distributions in some mammalian bones but without any clear dependence on vessel orientation, as suggested by qualitative observations. Examples include the matrix of the unremodeled (no secondary osteons) or poorly remodeled (few secondary osteons) bone in the opposing cortices ('tension cortex' vs. 'compression cortex') in the distal diaphysis of adult equine radii (Mason et al. 1995), the mid diaphysis of sub-adult ovine radii (Skedros & Kuo, 1999), and the mid diaphysis of sub-adult turkey ulnae (Skedros & Hunt, 2004). These examples suggest that it may be possible to draw broad comparisons in CFO-related histomorphological data between species and/or bones that otherwise might seem dissimilar and regardless of their capacity to form secondary osteons. However, to adequately test the hypothesis that variations in CFO might be more important than variations in LI for identifying tissue-level strain-mode-related adaptations for bending vs. torsion requires quantifying both characteristics in samples of bones of many avian species. We are aware of only two studies that have considered this issue (Skedros & Hunt, 2004; de Margerie et al. 2005). However, Skedros & Hunt (2004) only examined ulnae of domesticated turkeys and, although de Margerie et al. (2005) examined many bones in many avian species, they only roughly estimated LI. Experimental studies are needed that examine the independent influences of CFO and laminarity, and which of these characteristics is proximate in causing strain-mode-related adaptation.

In their study of many species of birds, de Margerie et al. (2005) considered the possibility that CFO and vascular orientations could be directly determined by the ratio between longitudinal (L) and 'diametric' (D; growth radially) rates of growth of the long bones. In this context, the L/D ratio represents the longitudinal/diametric growth rate ratio during morphogenesis. This follows a classical idea that tension and stretch in the periosteum determine the primary bone microstructure (Taylor, 1992; Lee, 2004; Warsaw et al. 2017). They examined the results of correlations obtained between L/D of adult long bones and CFO and estimated laminarity. Only weak correlations were found: $r = -0.22$ for L/D vs. CFO; and $r = -0.10$ for L/D vs. estimated LI. They argued that a much stronger influence of L/D

would have been found if L/D growth rate ratio actually was the direct cause of collagen and vascular orientation. By contrast, and in terms of bat vs. bird structural and histomorphological comparisons, Lee & Simons (2015) state that: (i) vascularity in birds and bats is best explained by higher somatic growth rates in birds; and (ii) because of absence of laminar bone in bats, and its presence in birds, suggests that it is not a necessary biomechanical feature in flying vertebrates and may be apomorphic to birds. Clearly, the relative importance of ontogenetic influences and phylogenetic factors remains unsettled.

Strain reversal in the dorsal-ventral direction in B3M

Our results showing similar WMGL-CFO in the opposing cortices in the habitual dorsal-ventral bending plane of the B3M can be explained by the lack of true 'tension' and 'compression' regions on opposite sides of the diaphyseal location that we analyzed. *In vivo* strain data obtained on the B3M during typical wing flapping show that it habitually experiences a reversal of strain mode, which imparts high compression followed by high tension to the dorsal and ventral cortices at different times (Swartz & Middleton, 2008). Equivalent tension and compression strain magnitudes within each of the opposing cortices along the direction of habitual bending is highly unusual when compared with all other habitually bent bones that have been studied histologically. To our knowledge, the strain mode and strain magnitude distributions are stereotypically/habitually non-uniform (compression > tension) in nearly all other bones studied in this context. However, this reflects a bias based on the preponderance of data being obtained from terrestrial locomotion. In contrast to the large majority of bones studied to date in terrestrial animals, more uniform strain distributions in the plane of bidirectional (single-plane) bending would likely be seen in most wings, flippers and fins. The 'exceptional case' of the strain reversals in the B3M likely explains the uniformity of CFO-WMGL, FASB and cortical thickness along this plane of habitual bending oscillations. While these findings in the B3M do not reject the hypothesis that patterns of CFO are highly sensitive to strain mode, they show that uniformity in CFO throughout a bone's cross-section does not always reflect habitual torsional loads.

Additionally in the B3M, the distribution and amount of secondary osteonal bone did not correspond to expected differences between the habitual dorsal-ventral bending direction and neutral axis (cranial-caudal cortices), and the distribution of bone did not appear to either enhance or resist bending in a particular direction. Based on available data in other species, the magnitudes of the regional variations in On.Ar and in the number and fractional area of secondary osteons that we found in the bat bones are likely also insufficient for significantly influencing regional mechanical properties (Skedros et al. 2013a). Consequently,

it seems likely that these variations reflect remodeling activities in earlier growth and/or remodeling activities associated with asymmetric soft tissue insertions.

FASB and OPD in ontogeny and for microdamage repair, and their potential relationships with cross-sectional robustness and body size

The higher FASB in the B3M when compared with the bat humerus might reflect the generally increased strain magnitudes, reduced bone size and the increased microdamage repair that likely occurs toward the distal end of the wing (Papadimitriou et al. 1996; Swartz & Middleton, 2008; Frongia et al. 2018). Hence, the functional loading environment of the more distal portion of the bat wing, especially because of its high morphing ability (i.e. the ability to change the shape of the wing that is not seen in birds; Hedenström & Johansson, 2015), requires modifications of the skeletal elements, especially via the osteonal remodeling process. In their histomorphological study of fluoro-chrome-labeled limb bones of bats of the same species examined by us, Bennett & Forwood (2010) also showed that the osteonal remodeling was '... predominantly quiescent [in adults, suggests] that remodeling had occurred in an early stage of life, possibly when the wings were being exercised in preparation for anticipated flight'. This observation helps to explain why we also found secondary osteons typically in the deeper regions of the bat bone cortices (i.e. closer to the medullary canal where the bone formed when the animals were younger). As suggested by the distributions of osteons shown in Fig. 1 (e.g. regional clusters deeper in the bone), there are also likely influences of cortical drift during growth. The formation of secondary osteons could also be related to remodeling observed during hibernation and lactation in these animals (Whalen et al. 1972; Doty & Nunez, 1985; Kwiecinski et al. 1987). We could not investigate any of these possibilities because only adult bones were used.

The absence of secondary osteons in the pigeon humerus, and in many avian and some mammalian limb bones of species with small body sizes lead to the question: Do these bones completely lack a mechanism for the intra-cortical repair of microdamage (assuming that microdamage occurs)? There are data from ulnae of adult laboratory rats, which rarely exhibit naturally occurring secondary osteon formation, showing that experimentally induced small crack damage in bone can be repaired without bone remodeling (Seref-Ferlengez et al. 2014). This important finding suggests that alternative repair mechanisms exist in bone to deal with submicron-sized matrix cracks should they occur in some natural conditions or circumstances. Consequently, bones like pigeon humeri that do not exhibit intracortical osteon-mediated microdamage repair do not mean that intracortical repair is not possible. Currey et al. (2017) speculate that because the cortices of the limb bones are so thin

in small-bodied mammals and birds (e.g. mice and sparrow-sized birds), they probably could not accommodate the holes produced by the remodeling process. This is because, even though the resorption cavities are temporary, the bones would be prone to rapid failure. This likely also applies to the bones examined in the present study, especially the pigeon humerus that had the thinnest cortex (and lacked secondary osteons). Whether or not the presence of osteons correlates with bone size is an important question that would require examining bones from bats that have the same body size of common pigeons. Support for this possibility is the observation of Lee & Simons (2015) that there appears to be a threshold of body size in adult bats (~ 100–200 g) above which vascularization occurs in their limb bones. However, because they did not examine bats in the 200–900 g size range suggests that more studies are needed to test this hypothesis.

In vivo strain data from pigeon and bat humeri show that their neutral axes shift broadly throughout the different stages of flight (up to ~ 40°), which results in relatively diffusely distributed shear stresses when compared with bones receiving habitual bending (Swartz et al. 1992; Biewener & Dial, 1995). The relatively high *K*-values (i.e. thin cortices) of these humeri (when compared with typical limb bones in non-flying animals; Currey & Alexander, 1985), their lack of regional variations in CFO, and the lack of obviously mechanically adaptive secondary osteon distributions (in bat humeri) might only partially represent shear-related adaptation. This set of characteristics is likely also influenced by circumstances where the requirements that favor a thin cortex relegate material adaptation to a subsidiary role when compared with structural adaptations in accommodating habitual loading conditions. This has been considered in terms of the 'cortical robusticity threshold hypothesis' (more likely at play in the bat and pigeon humeri) and/or the 'stressed volume effect' (possibly at play in all three bones; Skedros, 2011, 2012). These concepts suggest that there may be a threshold where the cortex is so thin that adaptations are mainly derived from structural characteristics and are comparatively minimally influenced by material characteristics (e.g. osteons and CFO). If this hypothesis is correct, then it might question the interpretation of our findings because the paradigm that intracortical histomorphological variations reflect adaptations in limb bone diaphyses might not apply to bones with very thin cortices. If this is true, then it suggests that the paradigm in which we couched our hypotheses regarding tissue-level adaptations is not concordant with that used in our prior studies of relatively more robust and/or larger bones — where predominant CFO and secondary osteons are expected to exhibit patterns that accommodate the strain distribution engendered by a bone's load history, especially for the stark differences in bending vs. torsion (Skedros, 2012). Hence, the lack of expected regional variation in structural and material characteristics (see Table 1, predictions 7–11) suggests that these

are not informative traits to measure in this system. This line of reasoning might help explain some cases where bone microstructure does not reflect conventional expectations (Lad et al. 2016) and has been applied to the thin-walled human femoral neck, which has clinical, biomechanical and evolutionary relevance (Skedros et al. 2016a). This is because the strain milieu caused by habitual loading of the femoral neck region, and changes in this loading with supraphysiological stresses and during advanced aging, has bearing on the etiology of stress and fragility fractures, and the origins and ontogenetic maintenance of cortical/cancellous organization and mass of this region (Mayhew et al. 2005; Lee et al. 2009; Ruff & Higgins, 2013; Reeve & Loveridge, 2014; Oliveira et al. 2016; Tang et al. 2018).

Load predictability: expected structural differences distinguishing bending vs. torsion were not found

Most of the expected structural differences between the B3M and the humeri were not found. For example, in the B3M the distribution bone was not mostly orthogonal to its habitual bending plane, which would have been best for enhancing load predictability as seen in bones with cross-sectional shapes like mid diaphyseal radii of horses and artiodactyls (Bertram & Biewener, 1988; Skedros, 2012). The distribution of bone was also not preferentially in the direction of habitual bending, which is sometimes how a habitually bent bone is arranged in some comparatively shorter bones like equine and artiodactyl calcanei (Skedros, 2012). What might explain the lack of asymmetry in the cross-section geometry of the B3M is that the *in vivo* strain data currently available for the B3M failed to detect episodes of more complex or torsional loading during less common wing motions. If this possibility is correct, then it is conceivable that only a few cycles of multidirectional/complex loads could be sufficient for producing shear-related adaptations, and hence the lack of regional structural and material variations. This idea is referred to as the 'shear-resistance priority hypothesis' (Skedros, 2012; Warshaw et al. 2017). Notably, the *in vivo* strain data of Swartz & Middleton (2008) were obtained while the bats flew only at moderate, steady speed, with no ascent or descent, and no turns or maneuvers. More extreme locomotor behavior would be expected to not only increase strain magnitudes but also increase load complexity, which increases the prevalence of shear strains (Keenan et al. 2017). However, to some extent our findings in the B3M may simply be a case where the more obvious structural adaptations seen in other bones (e.g. equine and artiodactyl calcanei and radii) are not required for load predictability. This is supported by the fact that the B3M functions comparatively less independently when compared with other limb bones studied thus far because the B3M is one of several bones within a distal portion of a complex wing structure that is designed for compliance (especially distally; Papadimitriou et al. 1996;

Swartz & Middleton, 2008; Hedenström & Johansson, 2015). This, when coupled with the high morphing ability of the bat wing, likely results in reduced load predictability of the bones during some common functional activities. Additional studies of *in vivo* strain magnitudes and distributions during various wing-flapping activities are needed to more fully understand the load histories of wing bones in bats and birds (e.g. as has been done in domesticated turkeys; Adams et al. 1997).

Conclusions

No differences in CFO were found between the dorsal and ventral cortices of the B3M despite *in vivo* strain data showing that these cortices are on opposing sides of a neutral axis. We argue that this reflects the strain reversals that place each of these cortices in equivalent magnitudes and durations of tension and compression in different portions of the wing-flapping cycle. Although the B3M has relatively greater CA/TA than the bat and pigeon humeri, it is quasi-circular with I_{max}/I_{min} between that of these humeri. Hence, like the pigeon and bat humeri, the B3M does not have clear structural adaptations for habitual bending in a single plane. The B3M therefore differs from many habitually bent bones studied previously, reflecting design features for enhanced flexibility at the distal end of a wing with complex structure and function. Consequently, one of the main findings of our study is that relatively uniform CFO throughout a bone's cross-section does not always reflect habitual torsional loads. Osteon morphology and distribution, and presence of laminar histology also do not distinguish torsion from bending in these bat and pigeon wing bones.

Acknowledgements

The authors thank Roy Bloebaum and Pat Campbell for laboratory support, Adam Beckstrom for technical work, and Sharon Swartz, Ron Shahar and Maitena Dumont for their critical reviews of the manuscript. Sharon Swartz provided the bat bones used in this study. Gregory Stoddard assisted with statistical analyses. Support for this research included medical research funds of the United States Department of Veterans Affairs medical research funds and a grant from the Orthopaedic Research and Education Foundation (OREF grant no. 01-024).

Conflict of interest

The authors have no conflict of interest to declare.

References

Adams DJ, Spirt AA, Brown TD, et al. (1997) Testing the daily stress stimulus theory of bone adaptation with natural and experimentally controlled strain histories. *J Biomech* **30**, 671–678.

- Almany Magal R, Reznikov N, Shahar R, et al. (2014) Three-dimensional structure of minipig fibrolamellar bone: adaptation to axial loading. *J Struct Biol* **186**, 253–264.
- Bender R, Lange S (2001) Adjusting for multiple testing—when and how? *J Clin Epidemiol* **54**, 343–349.
- Bennett MB, Forwood MR (2010) Histomorphometric changes in the wing bones of the fruit bat, *Pteropus poliocephalus*, (*Megachiroptera: Pteropidae*) in relation to increased bone strain and the failure of a good (?) hypothesis. *Aust Zool* **35**, 341–348.
- Bertram JE, Biewener AA (1988) Bone curvature: sacrificing strength for load predictability? *J Theor Biol* **131**, 75–92.
- Biewener AA, Dial KP (1995) *In vivo* strain in the humerus of pigeons (*Columba livia*) during flight. *J Morphol* **225**, 61–75.
- Bloebaum RD, Skedros JG, Vajda EG, et al. (1997) Determining mineral content variations in bone using backscattered electron imaging. *Bone* **20**, 485–490.
- Boyde A, Riggs CM (1990) The quantitative study of the orientation of collagen in compact bone slices. *Bone* **11**, 35–39.
- Bromage TG, Goldman HM, McFarlin SC, et al. (2003) Circularly polarized light standards for investigations of collagen fiber orientation in bone. *Anat Rec* **274B**, 157–168.
- Cubo J, Casinos A (1998) Biomechanical significance of cross-sectional geometry of avian long bones. *Eur J Morphol* **36**, 19–28.
- Currey JD (2002) *Bones: Structure and Mechanics*. Princeton, NJ: Princeton University Press.
- Currey JD, Alexander RM (1985) The thickness of the walls of tubular bones. *J Zool Lond* **206**, 453–468.
- Currey JD, Dean MN, Shahar R (2017) Revisiting the links between bone remodelling and osteocytes: insights from across phyla. *Biol Rev Camb Philos Soc* **92**, 1702–1719.
- Dmitrienko A, Tamhane AC, Bretz R (2010) *Multiple Testing Problems in Pharmaceutical Sciences*, pp. 4–7. New York, NY: CRC Press.
- Doty SB, Nunez EA (1985) Activation of osteoclasts and the repopulation of bone surfaces following hibernation in the bat, *Myotis lucifugus*. *Anat Rec* **213**, 481–495.
- Dunnnett C, Goldsmith C (2006) When and how to do multiple comparisons. In: *Statistics in the Pharmaceutical Industry*, 3rd edn (eds Buncher CR, Tsay J-Y), pp. 421–452. New York, NY: Chapman & Hall/CRC.
- Ebacher V, Tang C, McKay H, et al. (2007) Strain redistribution and cracking behavior of human bone during bending. *Bone* **40**, 1265–1275.
- Emmanuel J, Hornbeck C, Bloebaum RD (1987) A polymethyl methacrylate method for large specimens of mineralized bone with implants. *Stain Technol* **62**, 401–410.
- Enlow DH, Brown SO (1957) A comparative study of fossil and recent bone tissues. Part II. Reptilian and bird bone tissues. *Tex J Sci* **9**, 186–214.
- Foote JS (1916) *A Contribution to the Comparative Histology of the Femur*. Baltimore, MD: Lord Baltimore Press, Smithsonian Institution Washington.
- Francillon-Vieillot H, de Buffrénil V, Castanet J, et al. (1990) Microstructure and mineralization of vertebrate skeletal tissues. In: *Skeletal Biomineralization: Patterns, Processes and Evolutionary Trends* (ed. Carter J), pp. 471–530. New York, NY: Van Nostrand Reinhold.
- Frongia GN, Muzzeddu M, Mereu P, et al. (2018) Structural features of cross-sectional wing bones in the griffon vulture (*Gyps fulvus*) as a prediction of flight style. *J Morphol* **279**, 1753–1763.

- Hedenström A, Johansson LC (2015) Bat flight: aerodynamics, kinematics and flight morphology. *J Exp Biol* **218**, 653–663.
- Hintze J (2015) *NCSS 10 Statistical Software*. Kaysville, UT: NCSS, LLC.
- Hofmann R, Stein K, Sander PM (2014) Constraints of the lamina density of laminar bone architecture of large-bodied dinosaurs and mammals. *Acta Palaeontol Pol* **59**, 287–294.
- Keenan KE, Mears CS, Skedros JG (2017) Utility of osteon circularity for determining species and interpreting load history in primates and nonprimates. *Am J Phys Anthropol* **162**, 657–681.
- Kwieceński GG, Krook L, Wimsatt WA (1987) Annual skeletal changes in the little brown bat, *Myotis lucifugus lucifugus*, with particular reference to pregnancy and lactation. *Am J Anat* **178**, 410–420.
- Lad SE, Daegling DJ, McGraw WS (2016) Bone remodeling is reduced in high stress regions of the cercopithecoid mandible. *Am J Phys Anthropol* **161**, 426–435.
- Lee AH (2004) Histological organization and its relationship to function in the femur of *Alligator mississippiensis*. *J Anat* **204**, 197–207.
- Lee AH, Simons EL (2015) Wing bone laminarity is not an adaptation for torsional resistance in bats. *PeerJ* **3**, e823.
- Lee T, Choi JB, Schafer BW, et al. (2009) Assessing the susceptibility to local buckling at the femoral neck cortex to age-related bone loss. *Ann Biomed Eng* **37**, 1910–1920.
- Marelli CA, Simons EL (2014) Microstructure and cross-sectional shape of limb bones in Great Horned Owls and Red-tailed Hawks: how do these features relate to differences in flight and hunting behavior? *PLoS One* **9**, e106094.
- de Margerie E (2002) Laminar bone as an adaptation to torsional loads in flapping flight. *J Anat* **201**, 521–526.
- de Margerie E, Cubo J, Castanet J (2002) Bone typology and growth rate: testing and quantifying 'Amprino's rule' in the mallard (*Anas platyrhynchos*). *C R Biol* **325**, 221–230.
- de Margerie E, Robin JP, Verrier D, et al. (2004) Assessing a relationship between bone microstructure and growth rate: a fluorescent labelling study in the king penguin chick (*Aptenodytes patagonicus*). *J Exp Biol* **207**, 869–879.
- de Margerie E, Sanchez S, Cubo J, et al. (2005) Torsional resistance as a principal component of the structural design of long bones: comparative multivariate evidence in birds. *Anat Rec A Discov Mol Cell Evol Biol* **282**, 49–66.
- Mason MW, Skedros JG, Bloebaum RD (1995) Evidence of strain-mode-related cortical adaptation in the diaphysis of the horse radius. *Bone* **17**, 229–237.
- Mayhew PM, Thomas CD, Clement JG, et al. (2005) Relation between age, femoral neck cortical stability, and hip fracture risk. *Lancet* **366**, 129–135.
- Mears CS, Keenan KE, Kithas AA, et al. (2014) Recognizing and resolving inconsistencies and inaccuracies in determining osteon circularity: can methods be standardized? *Am J Phys Anthropol* **153**, 183.
- Mears CS, Litton SM, Phippen CM, et al. (2015) Improving accuracy, precision, and efficiency in analysis of osteon cross-sectional shape. *Am J Phys Anthropol* **154**, 223.
- Oliveira US, Labronici PJ, Joao Neto A, et al. (2016) Bilateral stress fracture of femoral neck in non-athlete – case report. *Rev Bras Ortop* **51**, 735–738.
- Papadimitriou HM, Swartz SM, Kunz TH (1996) Ontogenetic and anatomic variation in mineralization of the wing skeleton of the Mexican free-tailed bat, *Tadarida brasiliensis*. *J Zool Lond* **240**, 411–426.
- Pratt IV, Johnston JD, Walker E, et al. (2018) Interpreting the three-dimensional orientation of vascular canals and cross-sectional geometry of cortical bone in birds and bats. *J Anat* **232**, 931–942.
- Rasband W (1997–2016) *ImageJ*. Bethesda, MD: US National Institutes of Health.
- Reeve J, Loveridge N (2014) The fragile elderly hip: mechanisms associated with age-related loss of strength and toughness. *Bone* **61**, 138–148.
- de Ricolès A, Meunier FJ, Castanet L, et al. (1991) Comparative microstructure of bone. In: *Bone* (ed. Hall BK), pp. 1–78. Boca Raton, FL: CRC Press.
- Ruff CB (2002) Long bone articular and diaphyseal structure in old world monkeys and apes. I: locomotor effects. *Am J Phys Anthropol* **119**, 305–342.
- Ruff CB, Higgins R (2013) Femoral neck structure and function in early hominins. *Am J Phys Anthropol* **150**, 512–525.
- Sankoh AJ, Huque MF, Dubey SD (1997) Some comments on frequently used multiple endpoint adjustment methods in clinical trials. *Stat Med* **16**, 2529–2542.
- Seref-Ferlengez Z, Basta-Pljakic J, Kennedy OD, et al. (2014) Structural and mechanical repair of diffuse damage in cortical bone *in vivo*. *J Bone Miner Res* **29**, 2537–2544.
- Simons EL, O'Connor M (2012) Bone laminarity in the avian forelimb skeleton and its relationship to flight mode: testing functional interpretations. *Anat Rec (Hoboken)* **295**, 386–396.
- Skedros JG (2011) Collagen fiber orientation (CFO) variations in the hominid femoral neck are likely invalid for deciphering load history when cortical robusticity is low. *Am J Phys Anthropol* **552**, 275–276.
- Skedros JG (2012) Interpreting load history in limb-bone diaphyses: important considerations and their biomechanical foundations. In: *Bone Histology: an Anthropological Perspective* (eds Crowder C, Stout S), pp. 153–220. Boca Raton, FL: CRC Press.
- Skedros JG, Hunt KJ (2004) Does the degree of laminarity mediate site-specific differences in collagen fiber orientation in primary bone? An evaluation in the turkey ulna diaphysis. *J Anat* **205**, 121–134.
- Skedros JG, Kuo TY (1999) Ontogenetic changes in regional collagen fiber orientation suggest a role for variant strain stimuli in cortical bone construction. *J Bone Miner Res* **14**, S441.
- Skedros JG, Mason MW, Nelson MC, et al. (1996) Evidence of structural and material adaptation to specific strain features in cortical bone. *Anat Rec* **246**, 47–63.
- Skedros JG, Hunt KJ, Bloebaum RD (2004) Relationships of loading history and structural and material characteristics of bone: development of the mule deer calcaneus. *J Morphol* **259**, 281–307.
- Skedros JG, Dayton MR, Sybrowsky CL, et al. (2006) The influence of collagen fiber orientation and other histocompositional characteristics on the mechanical properties of equine cortical bone. *J Exp Biol* **209**, 3025–3042.
- Skedros JG, Sorenson SM, Hunt KJ, et al. (2007a) Ontogenetic structural and material variations in ovine calcanei: a model for interpreting bone adaptation. *Anat Rec* **290**, 284–300.
- Skedros JG, Sorenson SM, Jensen NH (2007b) Are distributions of secondary osteon variants useful for interpreting load history in mammalian bones? *Cells Tissues Organs* **185**, 285–307.
- Skedros JG, Mendenhall SD, Kiser CJ, et al. (2009) Interpreting cortical bone adaptation and load history by quantifying osteon morphotypes in circularly polarized light images. *Bone* **44**, 392–403.

- Skedros JG, Kiser CJ, Keenan KE, et al.** (2011) Analysis of osteon morphotype scoring schemes for interpreting load history: evaluation in the chimpanzee femur. *J Anat* **218**, 480–499.
- Skedros JG, Keenan KE, Williams TJ, et al.** (2013a) Secondary osteon size and collagen/lamellar organization (“osteon morphotypes”) are not coupled, but potentially adapt independently for local strain mode or magnitude. *J Struct Biol* **181**, 95–107.
- Skedros JG, Knight AN, Clark GC, et al.** (2013b) Scaling of Haversian canal surface area to secondary osteon bone volume in ribs and limb bones. *Am J Phys Anthropol* **151**, 230–244.
- Skedros JG, Doutré MS, Brown EM, et al.** (2016a) Advancing understanding of femoral neck histomorphology and its relationship to load history: use of bat and pigeon humeri as models for adaptation for habitual torsion. *62nd Annual Meeting of the Orthopaedic Research Society*, **41**, 734.
- Skedros JG, Doutré MS, Weaver DJ** (2016b) Proximate mechanisms involved in the formation of secondary osteon morphotypes: important considerations and a putative role of primary cilia of osteoblasts and osteocytes. *Osteologie* **25**, 101–112.
- Spiesz EM, Kaminsky W, Zysset PK** (2011) A quantitative collagen fibers orientation assessment using birefringence measurements: calibration and application to human osteons. *J Struct Biol* **176**, 302–306.
- StataCorp** (2015) *Stata 14.1*. College Station, TX: StataCorp LP.
- Swartz SM, Middleton KM** (2008) Biomechanics of the bat limb skeleton: scaling, material properties and mechanics. *Cells Tissues Organs* **187**, 59–84.
- Swartz SM, Bennett MB, Carrier DR** (1992) Wing bone stresses in free flying bats and the evolution of skeletal design for flight. *Nature* **359**, 726–729.
- Tang T, Ebacher V, Crompton P, et al.** (2015) Shear deformation and fracture of human cortical bone. *Bone* **71**, 25–35.
- Tang T, Crompton PA, Guy P, et al.** (2018) Clinical hip fracture is accompanied by compression induced failure in the superior cortex of the femoral neck. *Bone* **108**, 121–131.
- Taylor JF** (1992) The periosteum and bone growth. In *Bone, Vol. 6: Bone Growth – A* (ed. Hall BK), pp. 21–52. Boca Raton, FL: CRC Press.
- Warshaw J, Bromage TG, Terranova CJ, et al.** (2017) Collagen fiber orientation in primate long bones. *Anat Rec (Hoboken)* **300**, 1189–1207.
- Whalen JP, Krook L, Nunez EA** (1972) A radiographic and histologic study of bone in the active and hibernating bat (*Myotis lucifugus*). *Anat Rec* **172**, 97–108.